'life as we know it'. Of course putative ecosystems that are only weakly coupled to the surface environment (for example, subsurface[32,33]) are not excluded by such observations.

Surface oceans of liquid water are unique in the Solar System; conceivably this is part of the reason that Earth is the only planet in the Solar System with abundant surface life. Similar spectroscopic methods, although without resolution of the disk, may be useful in examining planets of other stars for indigenous life, as has been suggested for O_2 by Owen.[34] Large filled-aperture or interferometric telescopes intended for investigating extrasolar planets, especially those of terrestrial mass, might incorporate into their design the wavelength range and spectral resolution that has proved useful in the present work. In the radio search for extraterrestrial intelligence (SETI), optimum transmission through interstellar space and plausible planetary atmospheres lies in the 1–3 GHz range, not the MHz range used here.

The Galileo mission constitutes an apparently unique control experiment on the ability of fly-by spacecraft to detect life at various stages of evolutionary development on other worlds in the Solar System. Although a similar opportunity arises in the summer 1999 Earth fly-by of the ESA/NASA Cassini spacecraft on its way to Saturn, there are, because of funding constraints, no plans to observe the Earth with Cassini. Although a great deal more exploration remains to be done before such conclusions can be considered secure, our results are consistent with the hypothesis that widespread biological activity now exists, of all the worlds in this Solar System, only on Earth. □

Received 17 February; accepted 14 September 1993.

1. Carlson, R. W. *et al. Space Sci. Rev.* **60,** 457–502 (1992).
2. Hord, C. W. *et al. Space Sci. Rev.* **60,** 503–530 (1992).
3. Belton, M. J. S. *et al. Space Sci. Rev.* **60,** 413–455 (1992).
4. Gurnett, D. A. *et al. Space Sci. Rev.* **60,** 341–355 (1992).
5. Lederberg, J. *Nature* **207,** 9–13 (1965).
6. Lovelock, J. *Nature* **207,** 568–570 (1965).
7. Lovelock, J. E. *Proc. R. Soc.* B**189,** 167–181 (1975).
8. Sagan, C. *Proc. R. Soc.* B**189,** 143–166 (1975).
9. Carlson, R. W., Arakelian, T. & Smythe, W. D. *Antarct. J. U.S.* (in the press).
10. Drossart, P. J. *et al. Planet. Space Sci.* (submitted).
11. Henderson, L. J. *The Fitness of the Environment: An Inquiry into the Biological Significance of the Properties of Matter* (Peter Smith, Gloucester, Mass., 1913).
12. von Zahn, U., Kumar, R. S., Neimann, H. & Prinn, R. in *Venus* Ch. 13 (eds Hunten, D. M., Colin, L., Donahue, T. M. & Moroz, V. I.) (Univ. of Arizona Press, Tucson, 1983).
13. Owen, T. in *Mars* Ch. 25 (eds Keiffer, H. H., Jakosky, B. M., Snyder, C. W. & Matthews, M. S.) (Univ. of Arizona Press, Tucson, 1992).
14. Walker, J. G. C. *Evolution of the Atmosphere* (Macmillan, New York, 1977).
15. Léger, A., Pirre, M. & Marceau, F. J. *Astr. Astrophys.* (in the press).
16. Lippincott, E. R., Eck, R. V., Dayhoff, M. O. & Sagan, C. *Astrophys. J.* **147,** 753–764 (1967).
17. Chameides, W. L. & Davis, D. D. *Chem. Engng. News* **60,** 38–52 (1992).
18. Hogan, K. B., Hoffman, J. S. & Thompson, A. M. *Nature* **354,** 181–182 (1991).
19. Lewis, J. S. & Prinn, R. G. *Planets and Their Atmospheres* (Academic, New York, 1984).
20. Bowker, D. E., Davis, R. E., Myrick, D. L., Stacy, K. & Jones, W. T. Ref. Publ. No. 1139 (NASA, Washington, 1985).
21. Kilston, S. D., Drummond, R. R. & Sagan, C. *Icarus* **5,** 79–98 (1966).
22. Sagan, C. & Wallace, D. *Icarus* **15,** 515–554 (1971).
23. Sagan, C. *et al.* in *Biology and the Exploration of Mars* Ch. 9 (eds Pittendrigh, C. S., Vishniac, W. & Pearman, J. P. T.) (Natn. Acad. Sci. Washington, 1966).
24. Shklovskii, I. S. & Sagan, C. *Intelligent Life in the Universe* (Holden Day, San Francisco, 1966).
25. Sullivan, W. T., Brown, S. & Wetherill, C. *Science* **199,** 377–388 (1978).
26. Chapman, S. *Proc. phys. Soc.* **43,** 483–501 (1931).
27. Fainberg, J. & Stone, R. G. *Space Sci. Rev.* **16,** 145–188 (1974).
28. Gurnett, D. A. *J. geophys. Res.* **79,** 4227–4238 (1974).
29. LaBelle, J., Trumann, R. A., Boehm, M. H. & Gewecke, K. *Radio Sci.* **24,** 725–737 (1989).
30. Keller, A. thesis, Univ. Iowa (1990).
31. Hines, C. O., Paghis, I., Hartz, T. R. & Fejer, J. A. *Physics of the Earth's Upper Atmosphere* (Prentice Hall, Englewood Cliffs, 1965).
32. Lederberg, J. & Sagan, C. *Proc. Natn. Acad. Sci. U.S.A.* **48,** 1473–1475 (1962).
33. Gold, T. *Proc. natn. Acad. Sci. U.S.A.* **89,** 6045–6049 (1992).
34. Owen, T. in *Strategies for the Search for Life in the Universe* (ed. Papagiannis, M.) 177–185 (Reidel, Dordrecht, 1980).

ACKNOWLEDGEMENTS. We are grateful to W. O'Neil, F. Fanale, T. Johnson, C. Chapman, M. Belton and other Galileo colleagues, as well as W. Sullivan, for encouragement and support; and to J. Lederberg, A. Léger, J. Lovelock, A. McEwen, T. Owen and J. Tarter for comments. This research was supported by the Galileo Project Office, Jet Propulsion Laboratory, NASA and by a grant from NASA's Exobiology Program.

Direct observation of kinesin stepping by optical trapping interferometry

Karel Svoboda*†, Christoph F. Schmidt*‡, Bruce J. Schnapp§ & Steven M. Block*‖

* Rowland Institute for Science, 100 Edwin Land Boulevard, Cambridge, Massachusetts 02142, USA
† Committee on Biophysics, Harvard University, Cambridge, Massachusetts 02138, USA
§ Department of Cell Biology, Harvard Medical School, Boston, Massachusetts 02115, USA

Do biological motors move with regular steps? To address this question, we constructed instrumentation with the spatial and temporal sensitivity to resolve movement on a molecular scale. We deposited silica beads carrying single molecules of the motor protein kinesin on microtubules using optical tweezers and analysed their motion under controlled loads by interferometry. We find that kinesin moves with 8-nm steps.

ENZYMES such as myosin, kinesin, dynein and their relatives are linear motors converting the energy of ATP hydrolysis into mechanical work, moving along polymer substrates: myosin along actin filaments in muscle and other cells; kinesin and dynein along microtubules. Motion derives from a mechanochemical cycle during which the motor protein binds to successive sites along the substrate, in such a way as to move forward on average[1–3]. Whether this cycle is accomplished through a swinging crossbridge, and how cycles of advancement are coupled to ATP hydrolysis, have been the subject of considerable debate[4–6]. *In vitro* assays for motility[7,8], using purified components interacting in well-defined experimental geometries, permit, in principle, measurement of speeds, forces, displacements, cycle timing and other physical properties of individual molecules, using native or mutant proteins[9–14].

‡ Present address: Department of Physics, University of Michigan, Ann Arbor, Michigan 48109, USA.
‖ To whom correspondence should be addressed.

Are there steps?

Do motor proteins make characteristic steps? That is, do they move forward in a discontinuous fashion, dwelling for times at

well-defined positions on the substrate, interspersed with periods of advancement? We define the step size, which may be invariant or represent a distribution of values, as the distance moved forwards between dwell states. (Here we use 'step size' in its physical sense, and not to mean the average distance moved per molecule of ATP hydrolysed, also termed the 'sliding distance'[4,9,11,15,18]. The latter corresponds to the physical step size, or an integral multiple thereof, in models in which ATP hydrolysis and stepping are tightly coupled.) If stepping occurs, the distributions of step sizes and dwell times will place constraints on possible mechanisms for movement.

The motor protein kinesin has advantages over myosin for physical studies, despite a comparative dearth of biochemical data. It can be made to move slowly, permitting better time-averaging of position, and it remains attached to the substrate for a substantial fraction of the kinetic cycle[12,13,19], reducing the magnitude of brownian excursions. Movement by single molecules of kinesin has been demonstrated[12,13], and kinesin can transport small beads, which provide high-contrast markers for motor position in the microscope[8]. Unlike actin filaments, microtubules are relatively rigid[20], and can be visualized by video-enhanced differential interference-contrast microscopy[21] (DIC). Finally, recombinant kinesin expressed in bacteria has been shown to move *in vitro*, paving the way for future study[14].

Significant technical difficulties nevertheless exist in measuring movements of single molecules. The motions occur on length scales of ångströms to nanometres and on timescales of milliseconds and less. To obtain the high spatial and temporal sensitivity required, we combined optical tweezers[22,23] with a dual-beam interferometer[24] to produce an 'optical trapping interferometer'. A laser, focused through a microscope objective of high numerical aperture, provides position detection and trapping functions simultaneously, and can produce controlled, calibratable forces in the piconewton range. Using this device, we captured silica beads with kinesin molecules bound to their surface out of a suspension and deposited them onto microtubules immobilized on a coverslip. We then observed the fine structure of the motion as beads developed load by moving away from the centre of the trap.

Our data provide evidence for steps under three sets of conditions. At moderate levels of ATP and low loads, kinesin movement was load-independent, and the relatively high speed, in combination with brownian motion, precluded direct visualization of steps. A statistical analysis of the trajectories, however, revealed a stepwise character to the motion. At saturating levels of ATP and high loads, or at low levels of ATP and low loads, (when movement is slowed mechanically or chemically), it was possible to see the abrupt transitions directly. We estimate the step size to be 8 nm, a distance that corresponds closely to the spacing between adjacent α-β tubulin dimers in the protofilament of the microtubule[25], suggesting that the elementary step spans one dimer.

Optical trapping interferometer

Polarized laser light is introduced at a point just below the objective Wollaston prism into a microscope equipped with DIC optics (Fig. 1*a*). The prism splits the light into two beams with orthogonal polarization: these are focused to overlapping, diffraction-limited spots at the specimen plane, and together they function as a single optical trap[23]. A phase object in the specimen plane inside the region illuminated by the two spots (the detector zone) introduces a relative retardation between the beams, so that when they recombine and interfere in the condenser Wollaston prism, elliptically polarized light results (Fig. 1*a*, left). The degree of ellipticity is measured by additional optics[24] and provides a sensitive measure of retardation, which changes during movement, passing through zero when the object exactly straddles the two spots (for example, a bead moved along a microtubule, as shown in Fig. 1*a*, right). For small excursions (out to ~150 nm), the output of the detector system is linear with displacement (Fig. 1*a*, inset).

Over most of its bandwidth, detector noise is at or below 1 Å/$\sqrt{\text{Hz}}$ (Fig. 1*b*). The response to a 100 Hz sinusoidal calibration signal of 1 nm amplitude (Fig. 1*b*, inset) shows this ångström-level noise. An optical trapping interferometer has advantages over conventional split-photodiode systems[26,27]. Because it is a non-imaging device, it is relatively insensitive to vibrations of the photodetector. Laser light levels ensure that detectors do not become shot-noise-limited. The detector zone can be repositioned rapidly within the microscope field of view. Because trapping and position-sensing functions are provided by the same laser beam, the two are intrinsically aligned. Finally, the arrangement does not interfere with the simultaneous use of conventional DIC imaging.

Trapping force can be calibrated in a number of ways[28–31]. Two independent methods were used here. A rapid, convenient method applicable for small excursions from the trap centre is to measure the thermal motion of an unbound, trapped bead (Fig. 1*c*). The optical trap behaves like a linear spring, so that dynamics correspond to brownian motion in a harmonic potential, which has a lorentzian power spectrum. Experimental spectra are well fitted by lorentzians, and the corner frequency provides the ratio of the trap spring constant to the frictional drag coefficient of the bead[32]. The latter is obtained from Stokes' law, after correction for the proximity of the coverslip surface[33]. This approach permits forces on individual beads to be characterized *in situ*, just before or after their use in motility assays. A second approach, useful for larger excursions, is to move the stage in a sinusoidal motion while recording bead displacement from the fixed trap position (details are given in Fig. 1 legend). Both methods give results agreeing within 10%.

Low-load regime

Silica beads were incubated with small amounts of kinesin, such that they carried fewer than one active molecule, on average, and were deposited on microtubules with the optical trap. The power was set to ~17 mW at the specimen plane, providing a nominal trapping force that varied linearly from 0 pN at the centre to ~1.5 pN at the edge of the detector zone (~200 nm). The ATP concentration was fixed at 10 μM. Mean bead velocity in the outermost region of the trap, corresponding to the greatest force, was within 10% of that measured near the trap centre (51 nm s^{-1} versus 54 nm s^{-1}). As observed previously[13], beads frequently released from the microtubule after a variable period of progress (runs) and were drawn rapidly back to the trap centre (within $\leqslant$2 ms), whereupon they rebound and began to move again (Fig. 2*a*). Multiple cycles of attachment, movement and release were observed, with the same bead passing repeatedly through the detector region (as many as 20 times). The points of release, hence the corresponding force levels, were not the same at each pass. Measurements were terminated when a bead travelled out of the trap altogether or became stuck.

Bead displacement during one run is shown in Fig. 2*b*. The thermal noise in the displacement signal decreased as the bead developed load and walked toward the edge of the trap (Fig. 2*c*), indicating a nonlinear elasticity. This can be explained as follows. The bead's position is determined by its linkage to two springs. The first is the optical trap, with spring constant k_{trap}. The second is the linkage connecting the bead to the microtubule, acting through the motor, with spring constant k_{motor}. Both springs are extended as the motor pulls forward. If these springs were linear, thermal motion would be independent of the equilibrium position, with a mean-square displacement given by $\langle x^2 \rangle = k_B T/(k_{\text{trap}} + k_{\text{motor}})$, where k_B is Boltzmann's constant and T is the temperature. Therefore, the data of Fig. 2*c* imply that k_{motor} gets stiffer with increased extension. It is this diminution of noise, in part, that makes it possible to see steps: when the amplitude of the thermal noise is substantially larger than the step size, steps cannot be detected by any of the methods

used here (our unpublished computer simulations). This underscores the need to keep the bead-to-motor linkage stiff in experiments designed to look for molecular-scale motion, and also for imposing a stiff external tension. Considerable variability was observed in the mean noise level from bead to bead in these experiments, as well as in the degree of noise reduction under tension (by factors of 1–3). For this reason, and because of the relatively large extension (tens of nanometres), we consider it unlikely that stretching of the kinesin molecule itself was chiefly responsible for nonlinear behaviour. One reasonable explanation

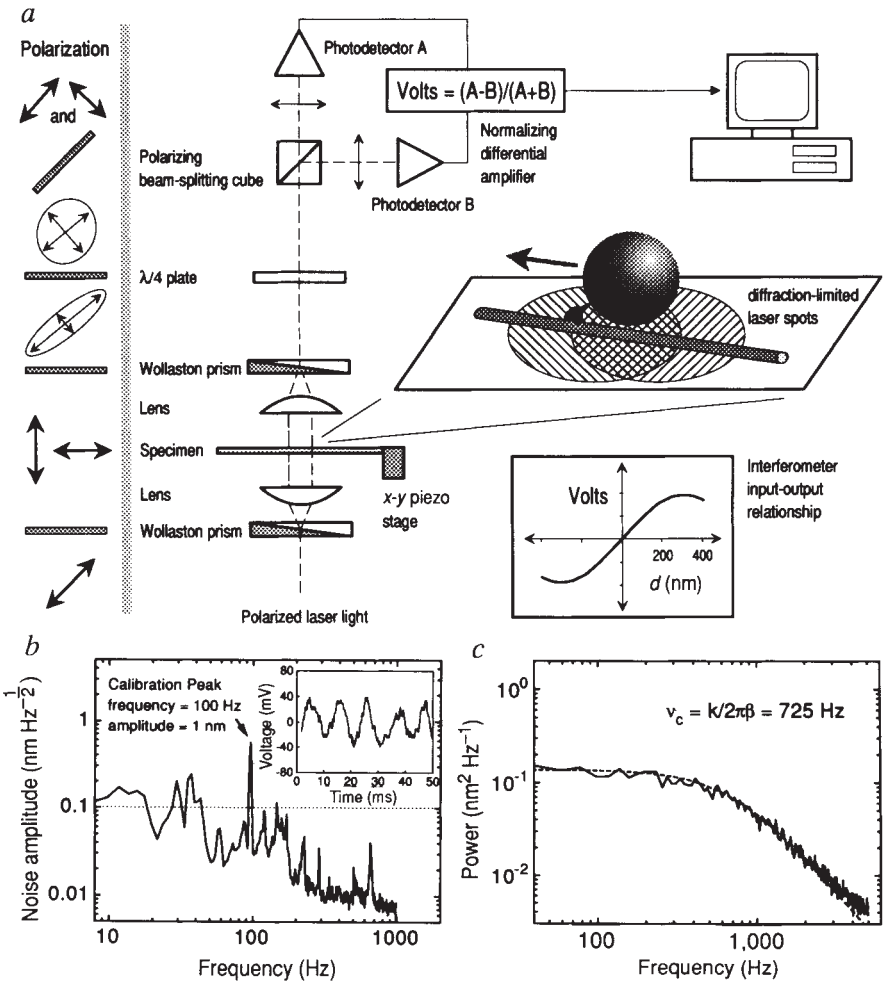

FIG. 1 The optical trapping interferometer. *a* (left), The diagram illustrates the polarization state of light as it passes through elements of the system, viewed along the optical axis. *a* (right), A schematic of the instrument. Polarized laser light passes through a Wollaston prism and is focused to two overlapping diffraction-limited spots (~1 μm diameter) with orthogonal polarization, separated by roughly ~250 nm. After passage through the specimen (a bead propelled along a microtubule by a kinesin molecule), light recombines in the upper Wollaston and develops slightly elliptical polarization (see text). Ellipticity is measured by a quarter waveplate, which produces nearly circularly polarized light, followed by a polarizing beam-splitting cube, which splits the light into two nearly equal components. The difference in intensity is detected by photodiodes and a normalizing differential amplifier. Signals were analysed offline (LabView, National Instruments). *b*, Sensitivity of the interferometer. The graph shows the spectral noise density of the interferometer responding to a 100-Hz calibration signal of 1-nm amplitude. The large peak (arrow) corresponds to the signal. The detector voltage output (inset) shows both signal and noise. *c*, Force calibration of the optical trap. The thermal noise spectrum of a bead trapped using 58 mW of laser power is shown (solid line). The spectrum is fitted by a lorentzian (dashed line).

METHODS. We used a modified inverted microscope (Axiovert 35, Carl Zeiss) equipped with Nomarski DIC optics (Plan Neofluar 100×/1.3NA oil objective) fixed to a vibration isolation table (TMC Corp.). Light from a Nd:YLF laser (CW, 3W TEM_{00}, $\lambda = 1{,}047$ nm; Spectra Physics) was coupled by an optical fibre. Beam-steering was accomplished with a telescope arrangement[13,23]. An *x*–*y* piezo stage (Physik Instrumente) allowed positioning of the specimen under computer control. To measure instrument noise, a bead was embedded in polyacrylamide to suppress brownian motion and introduced into the detector. The stage was moved in a sinusoidal motion along the *x* axis to provide a calibration signal while recording voltage, and the power spectrum was computed. The power spectrum was scaled by computing the integral under the calibration peak and setting this equal to the mean-square value of the sinusoidal displacement amplitude. To calibrate the trap stiffness, and thereby the force, a bead in solution was trapped (typically ~2 μm above the coverslip) and its brownian motion recorded, from which a power spectrum was computed. The corner frequency provides the ratio of trap stiffness to the viscous drag of the bead; drag was calculated from the bead's diameter and corrected for proximity to the coverslip. One-sided power spectra were normalized such that $\langle x^2 \rangle = \int_0^\infty S(f)\, df$, where $\langle x^2 \rangle$ is the mean-square displacement and $S(f)$ is the power at a given frequency. Trapping force changed by less than 10% as the distance from the coverslip was reduced from 2 to 1 μm (data not shown). The force profile of the trap was also mapped over a larger range of displacements by moving the stage in sinusoidal fashion (amplitude $A = 2.5$ μm at frequency f) while monitoring the peak displacement, y, of a bead. At low frequencies, the force exerted by the fluid is $F = 2\pi A\beta f = k_{trap} y$, where $\beta = 5.7 \times 10^{-6}$ pN s nm^{-1} is the drag coefficient of the bead. The proportionality between y and f gave the mean stiffness, $(4.3 \pm 0.3) \times 10^{-4}$ pN nm^{-1} mW^{-1}, which was approximately constant out to displacements of ±200 nm (data not shown). The foregoing stiffness was used to compute mean forces in the outermost regions of the trap. Power at the specimen plane was estimated by measuring the external power with a meter and applying an attenuation factor of 58%, corresponding to the transmittance of the objective at 1,064 nm, determined separately (data not shown). Kinesin was purified from squid optic lobe by microtubule affinity[47] and tubulin from bovine brain[48]. Experiments were done at room temperature. Silica beads (0.6 μm diameter, 6×10^{-6} w/v final concentration; Bangs Labs) were incubated for at least 5 min in buffer (80 mM PIPES, 1 mM $MgCl_2$, 1 mM EGTA, pH 6.9, 50 mM KCl, 0.5 mM dithiothreitol, 50 μg ml^{-1} filtered casein, 1–500 μM ATP, 0.5 μg ml^{-1} phosphocreatine kinase, 2 mM phosphocreatine; in some experiments, the last three reagents were replaced by 2 mM AMP-PNP). Beads were incubated for >1 h with kinesin diluted ~1:10,000 from stock (~50 μg ml^{-1} kinesin heavy chain). Taxol-stabilized microtubules were introduced into a flow chamber in which the coverslip had been treated with 4-aminobutyl-dimethylmethoxysilane (Huls America): microtubules bound tightly to this surface. The chamber was then incubated with 1 mg ml^{-1} casein (in 80 mM PIPES, 1 mM $MgCl_2$, 1 mM EGTA, pH 6.9) for 10 min, rinsed with buffer, and kinesin-coated beads introduced. Beads were captured from solution with the trap and deposited on a microtubule selected with its long axis parallel to the Wollaston shear direction, the direction of detector sensitivity. Fewer than half the beads bound and moved when placed on a microtubule. Under these conditions, beads carry Poisson-distributed numbers of functional motors[13]. The bead size in these studies was such that the chance that any bead carried two motors in sufficient proximity to interact simultaneously with the microtubule was less than 2%, assuming, generously, that kinesin heads can reach 100 nm from their points of attachment.

for the nonlinearity is that the bead–motor linkage behaves like an entropic spring, with the swivelling motion of the bead at the end of its tether contributing degrees of freedom. This linkage becomes taut under load, such that subsequent displacements of the motor are communicated sharply to the bead.

Beads under the conditions shown in Fig. 2*a*, *b* moved close to 50 nm s^{-1}. The speed and the thermal noise in the data made a statistical analysis necessary to detect periodic structure. We used the following approach. First, reduced-noise segments of all runs in an experiment were selected, corresponding to movements under load, and filtered to further reduce noise (see below). Then, a histogram of all pairwise differences in displacement was computed for each record[34]. This 'pairwise distance distribution function' (PDF) shows spatial periodicities in stepping motion, independent of times at which steps occur. Next, PDFs were averaged. Finally, the power spectrum of the average PDF was computed: this produces a peak at the mean spatial frequency of the stepper.

For a noiseless, stochastic stepper (equidistant advances after exponentially distributed time intervals), the PDF gives a set of evenly spaced peaks at multiples of the step distance. For noisy steppers, peaks become broadened, disappearing altogether when their peak widths (r.m.s. amplitudes of brownian motion) exceed the step size. The detection of steps in the presence of noise can be improved by low-pass filtering the records with an appropriate filter frequency so as to preserve stepwise character. For this purpose, we used a nonlinear median filter[35]. Computer simulations showed that the peak stepping signal recovered from a background of gaussian noise by an appropriately chosen median filter was approximately twice the amplitude of an equivalent, linear Bessel filter (our unpublished data).

The PDF and associated power spectrum for a single run along a microtubule are shown in Fig. 3*a*, *b*. Even in individual runs, there was often an indication of periodicity in the PDF, with a spacing from 6–8 nm, although there was considerable variation from run to run. Averaged data (Fig. 4*a*, *b*), gave peaks corresponding to an uncorrected spacing of 6.7 ± 0.2 nm (mean ± s.e.). Essentially identical data were obtained for beads moving on axonemes (data not shown). Note that backward movements, corresponding to negative distances in the PDF, were practically non-existent. Can our instrument, in combination with the analysis, reliably detect nanometre-sized steps in a noisy background? To test this, we attached beads carrying single motors to microtubules with AMP-PNP, a non-hydrolysable ATP analogue. Beads bound in rigor by AMP-PNP exhibited brownian motion but did not translocate. The piezo stage of the microscope was then stepped stochastically to move the entire specimen (bead and microtubule) through the detector zone, parallel to the long axis of the microtubule, in a series of 8-nm increments, at the same speed as the kinesin-based movement of Fig. 4*a*. The PDF and power spectrum for this experiment gave peaks at nearly the same positions (Fig. 4*c*, *d*). (Similarly, experiments with a stage moved in 4-nm increments gave peaks at half this spacing; data not shown.) Smaller, secondary peaks (measured relative to the sloping background) at subharmonics of the main spatial frequency are usually seen: these arise mainly from the variation in peak heights in the PDF. The measured periodicity was 6.5 ± 0.2 nm, a distance that is 19% smaller than the anticipated value (8 nm). The discrepancy is a consequence of stretching in the elastic bead–motor linkage under load, causing beads to move only a fraction of the motor displacement. (The fraction is $k_{motor}/(k_{trap}+k_{motor})$ for linear springs.) This interpretation was confirmed by an experiment with beads bound directly to the coverslip that had dramatically reduced brownian motion. When the stage was again stepped stochastically by 8 nm, we obtained a strong peak at 8.0 ± 0.2 nm (Fig. 4*e*, *f*). Therefore, applying a 19% correction to the spectrum of Fig. 4*b* yields an adjusted estimate of 8.3 ± 0.2 nm for the mean periodicity of kinesin-based movement.

Could the filtering and/or statistical analysis produce

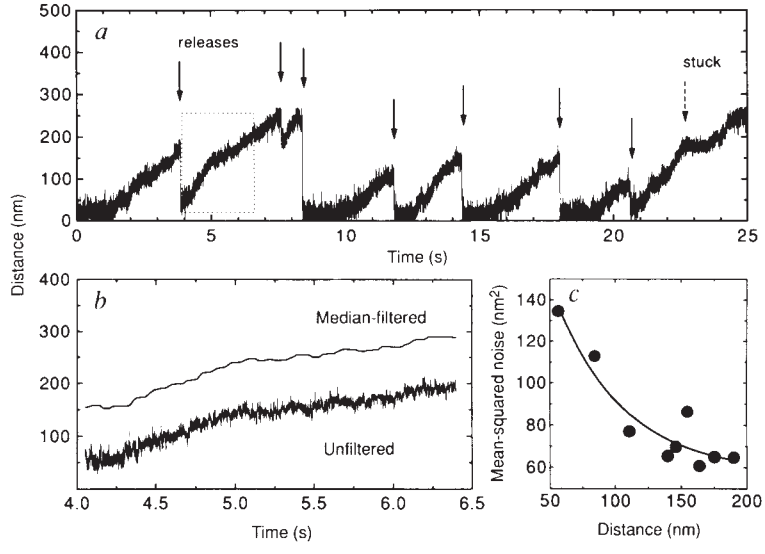

FIG. 2 *a*, Distance of a bead from the trap centre over 25 s. Multiple cycles of movement, release (solid arrows) and reattachment can be seen. The bead stuck briefly (<1 s) at 23 s (dashed arrow), then continued. The apparent peak between seconds 8 and 9 (third arrow) is a consequence of interferometer nonlinearity: the bead actually passed the turnover point in voltage at ~280 nm (Fig. 1*a*, inset) and continued its forward movement briefly before releasing. Portions of records beyong 200 nm were not analysed. *b*, Detail from the dashed box in *a*. The raw data (lower trace) were median-filtered for subsequent analysis (upper trace). *c*, The mean-square noise of the track in *b* as a function of distance from the trap centre. The noise decreases as the bead is placed under tension by the trap.

METHODS. Data were acquired at 1 kHz. A cubic polynomial was fitted to the response function (Fig. 1*a*, inset), and used to convert voltage to distance, a procedure that extended the usable instrument range to ±200 nm with a ±5% error (data not shown). The algorithm computes the absolute value of displacement, so that the distance from the centre of the trap is rectified. Record segments corresponding to movement near the trap centre were not used for analysis. The response function was determined by tracking the motion of beads stuck tightly to the coverslip surface and moved with computer-controlled voltage waveforms supplied to the piezo stage. The piezo stage was calibrated with nanometre-scale precision using video-based methods[38] against a 10-μm diamond-ruled grating (Donsanto Corp.). A calibration procedure was implemented that allowed beads of slightly varying size to be used, even though these scatter different amounts of light. This was made possible by the observation that the turnover point in the response function (Fig. 1*a*, inset) occurs at a fixed distance from the trap centre, independent of the bead size, and that the response function scales with voltage at that point. By measuring the turnover voltage, it was possible to establish an absolute correspondence between voltage and distance. Only runs longer than 100 nm were analysed for steps, as follows. A line was fitted to the run, and the slope used as a first estimate of velocity, v'. A set of non-overlapping segments of duration $2d/v'$ was then fitted to the run, where d is an assumed step size, and an improved estimate of velocity, $\langle v \rangle$, was computed from these segments. The filter frequency was chosen such that $f_c \approx 2\langle v \rangle/d$. Data were filtered with a Bessel filter at $1.2f_c$ and then by a median filter[35] of rank r, chosen such that $f_c = 1/(2r+1)$. This procedure was determined by computer simulations to provide reliable results with stochastic steppers subject to gaussian white noise. The exact choice of d is not critical: for the final data analysis, $d = 8$ nm was assumed, but other values (from 4 to 16 nm) gave essentially identical results. The noise in *c* is the mean-square deviation of unfiltered data from successive line segments.

artefactual results? To answer this question, we again bound beads to microtubules with AMP-PNP, but moved the specimen smoothly through the trap at the same mean speed. The PDF and associated power spectrum (Fig. 4*g*, *h*) had similar baselines, but no peaks corresponding to spatial periodicities. The variation in several such spectra provided a means of estimating the statistical significance of the peak in Fig. 4*b*: its likelihood of random occurrence is $P<0.00001$.

High-load regime

The laser power was set to ~58 mW at the specimen plane, a level that provided a nominal force that varied linearly from 0 pN at the centre to ~5 pN at the edge of the detector zone. The ATP concentration was raised to 500 μM (saturation level). When beads carrying single kinesin molecules were placed on microtubules, their motion was more erratic than at lower powers. Beads near the trap centre, experiencing low loads, moved rapidly at 300–500 nm s^{-1}. Under higher loads towards the edge of the trap, beads markedly slowed (or became stuck), although some were still able to escape altogether, opposing forces up to 5 pN. Other beads slowed or stuck before reaching the trap's edge, then continued forward at increased speed. Shuttering the trap briefly (<0.5 s) during a slow (or stuck) episode enabled some beads, but not all, to regain forward motion. Multiple transitions between fast- and slow-moving phases were seen in individual records, with beads entering the slow phase over a range of positions (loads) in the trap. Beads still underwent multiple cycles of movement, release and reattachment, similar to the behaviour observed at lower loads.

In the slow-moving phase, the reduced speed permitted visualization of steps. Figure 5*a*, *b* shows two records at high load, each containing roughly ten abrupt displacements forwards. The heights of these steps varied from ~5–18 nm, with the smaller transitions averaging 8 ± 2 nm (mean ± s.d.; $n=16$; Fig. 5*c*-*f*). Beads also advanced through what appeared to be 'double steps' (~17 nm), but it was not possible, given the bandwidth and noise in these signals, to determine whether such jumps represented two steps in rapid succession or one single step. Assuming that motors are stochastic steppers, one expects an exponential distribution of dwell times with numerous short steps. Records

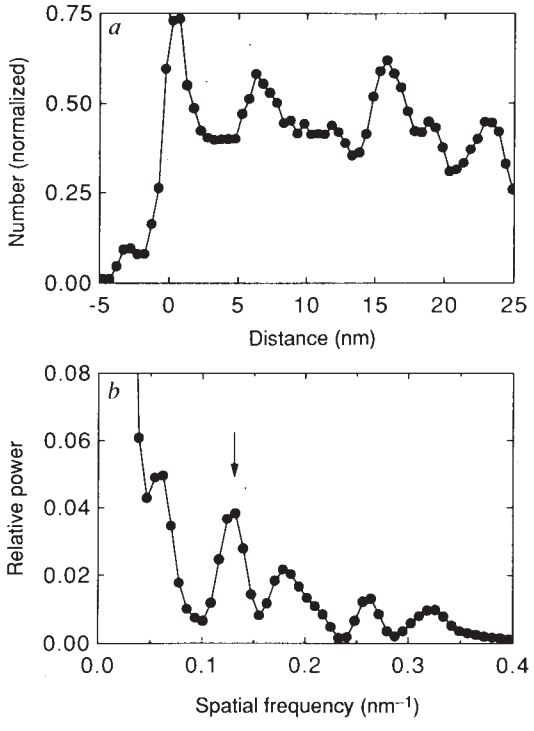

FIG. 3 *a*, The pairwise distance distribution function (PDF) for a single run. The density of interpoint distances in a median-filtered record is shown: multiple peaks with regular spacing can be identified. *b*, The normalized power spectrum of the data in *a*, showing a prominent peak at ~0.130 nm^{-1} (arrow), corresponding to periodicity of 7.7 nm.
METHODS. PDFs were computed by binning distance differences $(x_j - x_i)$ for all $(j>i)$ in a histogram, with bin width 0.5 nm. The PDF was normalized to unity at the first bin and smoothed wth a 3-point moving window. The one-sided power spectrum, $S(k)$, was computed from the PDF by FFT and normalized to unity at $S(0)$. The PDF is identical to the autocorrelation function of the density of distances from the trap centre. $S(k)$ is analogous to the square of the structure factor used in X-ray scattering, with the density of distances being analogous to electron density[49].

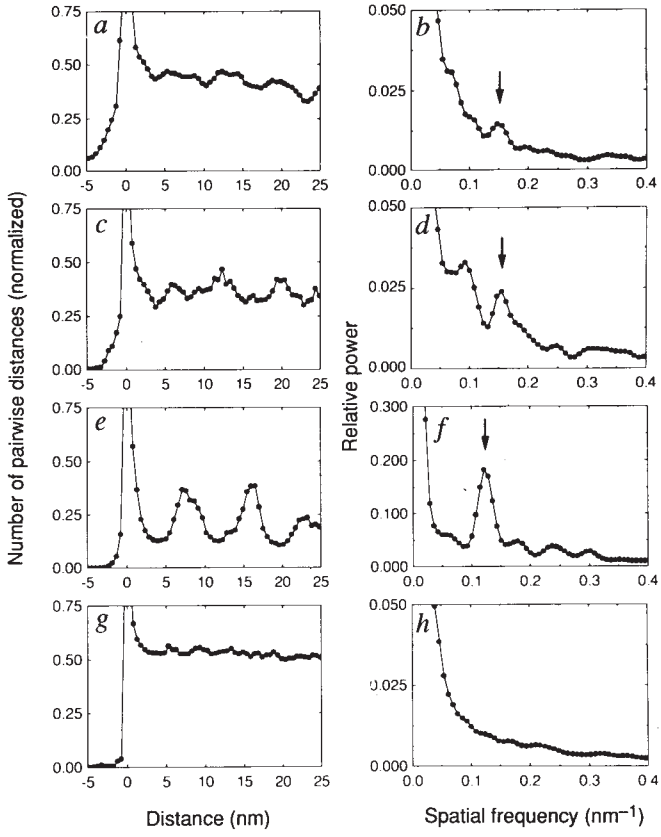

FIG. 4 *a*, The averaged pairwise distance distribution function (PDF) for kinesin movement, taken from 17 records of 10 different beads. *b*, The power spectrum of the data in *a*, with a peak at 0.149 ± 0.004 nm^{-1} (arrow), corresponding to a periodicity of 6.7 ± 0.2 nm. *c*, The averaged PDF for beads attached to the microtubule using AMP-PNP, with an 8-nm stochastically stepped stage. *d*. The power spectrum of the data in *c*, with a main peak at 0.154 ± 0.004 nm^{-1} (arrow), corresponding to a periodicity of 6.5 ± 0.2 nm. *e*, The averaged PDF for beads attached directly to the coverslip, with an 8-nm stochastically stepped stage. *f*, The spectrum of the data in *e*, with a peak at 0.125 ± 0.003 nm^{-1} (arrow), corresponding to a periodicity of 8.0 ± 0.2 nm. *g*, The averaged PDF for beads attached to the microtubule using AMP-PNP with a smoothly moved stage. *h*, The power spectrum of *g*. The average amplitude fluctuation about the mean for records of smooth movement was 0.002 units over the range of spatial frequencies 0.1–0.2; that is, there are no statistically significant peaks in this trace. All PDFs and power spectra were normalized to unity. Note different scale in *e*.
METHODS. PDFs in each panel represent averages of 17 records. Peak positions in power spectra and corresponding error estimates were determined by fitting gaussians. To estimate the statistical significance of the peak in *b*, the standard deviation per point, σ_k, for 17 spectra of individual runs of a smoothly stepped stage was computed. The likelihood of the peak was $\langle (S_k - \bar{N}_k)^2 \rangle^{1/2} / \langle \sigma_k \rangle$, where S_k is the average spectrum of kinesin-driven movement in *b*, and $\bar{N}_k$ is the average spectrum of smooth movement in *h*; averages were taken over the four spatial frequencies comprising the peak.

of the type shown in Fig. 5*a*, *b* are relatively hard to obtain: additional records must be collected before a more complete statistical analysis, including measurements of dwell-time distributions, will be possible. In parts of the record, the distance from the centre of the trap appeared to shorten briefly ($\sim$10 ms) just before a step (Fig. 5*e*, *f*), but this was not seen in all cases (Fig. 5*c*, *d*). We do not know if this behaviour reflects an intrinsic property of the motor, but the shortening is not due to kinesin unbinding because substrate release for periods as short as a millisecond would result in the bead being pulled off completely (Fig. 2).

Low-ATP regime

Reasoning that steps might also be resolved under low loads if beads moved slowly enough we restored the power to 17 mW and lowered the ATP concentration to 1 or 2 μM. When beads carrying single kinesin molecules were placed on a microtubule, their speeds were slow, about 5–15 nm s^{-1}, and single steps could again be seen in records that were selected for low noise (and therefore, presumably, stiffer bead–motor linkages) (Fig. 6*a*–*e*). A statistical analysis of these, like that performed in the low-load regime, showed that steps measured 8.2 ± 1.1 nm (mean ± s.d., as determined from peak positions in power spectra for all five panels), the same size as those seen in the high-load regime. Figure 6*f*, *g* shows an example of the PDF and associated power spectrum for the data of Fig. 6*e*, where the mean periodicity was 8.8 ± 0.5 nm.

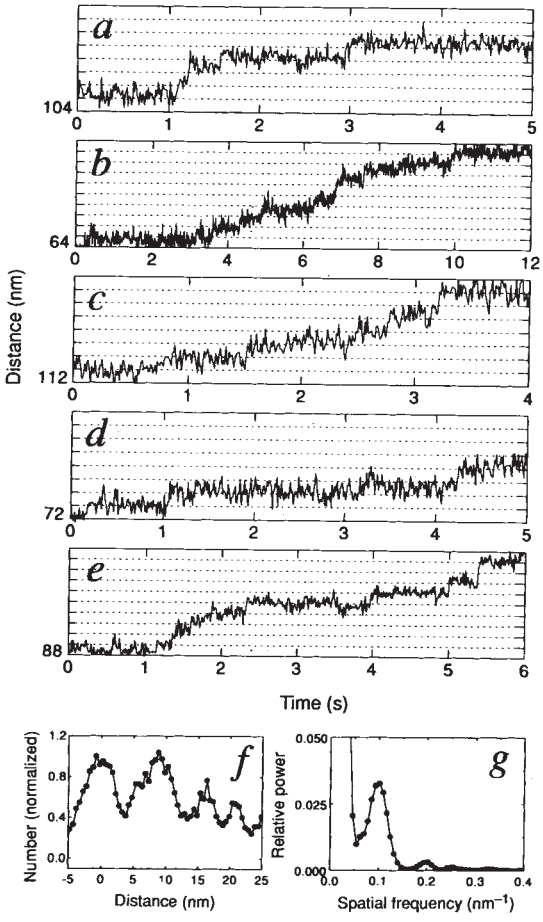

FIG. 6 *a*, *b*, Multiple steps in the displacement records of two different beads moving at an ATP concentration of 2 μM. *c*–*e*, Multiple steps in the displacement records of three different beads moving at an ATP concentration of 1 μM. Horizontal gridlines (dotted) have been drawn at a spacing of 8 nm. A 10-point jumping average of data taken at 1 kHz is plotted for an effective rate of 100 Hz. *f*, *g*, The PDF and associated power spectrum of the record in e, showing a periodicity of 8.8 ± 0.5 nm. Mean step size and s.d. for records in *a*–*e* were computed from peak positions determined from PDFs. A correction for the extension in k_{motor} has not been applied to these data, which were selected for their low noise and which presumably reflect stiffer linkages.

Is it possible that kinesin motors travel a longer, possibly variable, distance with each ATP hydrolysis, moving by some integral multiple of this spacing? That is, does a single hydrolysis result in a sequence of physical steps, rather than just one, as has been proposed for myosin[4,5,16,36] ? If this were the case for kinesin, then for extremely low concentrations of ATP (the diffusion limit), one would expect a motor to advance in a rapid burst of steps (through $\gg$8 nm) before stopping to wait for the next ATP molecule. This would produce motion characterized by periods of zero advancement interspersed with clusters of steps. The mean rate of advance during a step series ought to be high, close to the speed for saturating levels of ATP ($\sim$500 nm s^{-1}). We saw no evidence for step clusters in any of our records at 1 or 2 μM ATP: overall rates of advancement were quite uniform.

Discussion

The finding of discrete stepping behaviour should allow direct measurement of kinetic parameters of the mechanochemical cycle, by determining the timing of various phases of the motion. For example, releases of the type shown in Fig. 2*a* permit an estimate of the cycle off-time. Once a bead near the edge of the trap detaches under low load conditions, it is returned rapidly to the centre through a distance, x, of $\sim$200 nm within an average time $\tau = 1.8 \pm 0.4$ ms (mean ± s.e.). To make net forward progress, the kinesin off-time, τ_{off}, must be less than the time required for the trap to pull the bead back by one step, d, that is, $\tau_{off} < d/v = d\tau/x$, where v is the return speed at the edge of the trap. Using 8 nm for d gives $\tau_{off} \leqslant 72$ μs. This time is an upper limit, because velocity is practically unaffected by trapping forces. Such a short off-time signifies that kinesin somehow remains bound, sustaining load throughout most of its activity, perhaps moving hand-over-hand[12,37]. Estimates of other kinetic parameters are ongoing subjects of investigation.

It is known that kinesin motors do not wander over the surface lattice of a microtuble, but move instead along straight paths parallel to a protofilament[38–40]. Kinesin head fragments cloned from squid[41] or *Drosophila*[42] and expressed in bacteria have been used to decorate microtubules. Such fragments are non-functional in motility assays, but they bind microtubules and have microtubule-activated ATPase activity. Saturation binding experiments indicate a stoichiometry of one kinesin heavy-chain fragment to each tubulin dimer[42], and crosslinking studies demonstrate that it is the β-subunit of tubulin that is bound[41]. Electron microscopy of decorated microtubules shows an 8-nm repeat arising from the head spacing[41,42]. Taken together with our observations, this suggests that the two heads of a kinesin molecule walk along a single protofilament—or walk side-by-side on two adjacent protofilaments—stepping $\sim$8 nm at a time, making one step per hydrolysis (or perhaps fewer, requiring multiple hydrolyses per step). If the foregoing model is correct, then during movement of single molecules, the ATP hydrolysis rate, r_{ATP}, should be related to the step size, d, and speed, v, through $r_{ATP} = v/d$. Movement at saturating levels of ATP ($v \approx 500$ nm s^{-1} and even higher[20]) implies $r_{ATP} \geqslant 60$ s^{-1} mol^{-1}, 6–10-fold higher than reported[43–45]. The hydrolysis rates for motility assays *in vitro* must therefore be substantially higher than values inferred from solution biochemistry, or motors must make several steps per ATP hydrolysed. The latter is difficult to reconcile with our data, particularly at low concentrations of ATP.

Occasionally jumps have been seen[38] in selected records of kinesin movement during video tracking, measuring 3.7 ± 1.7 nm, although most of the movement was subjectively

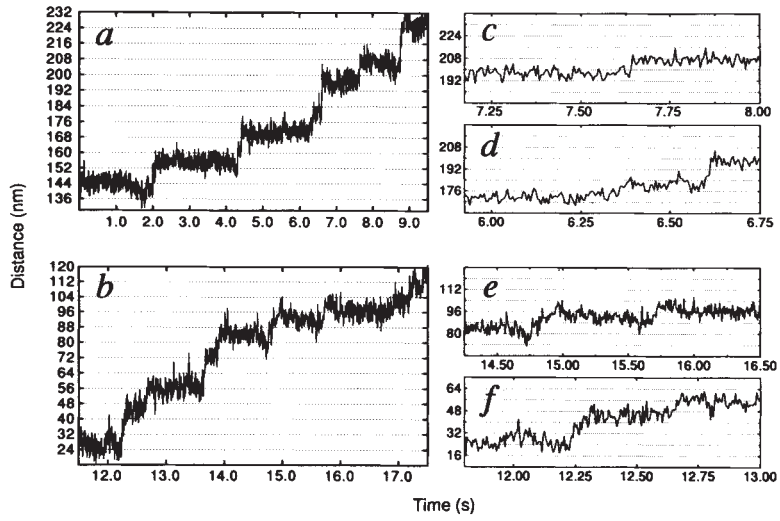

FIG. 5 *a*, *b*, Multiple steps in the displacement records of two different beads in the high-load regime. *c*, *d*, Details of selected steps in *a*. *e*, *f*, Details of selected steps in *b*. Horizontal gridlines (dotted) have been drawn at a spacing of 8 nm. A 5-point jumping average of data taken at 1 kHz is plotted for an effective rate of 200 Hz. The mean step size for these records was computed from averaged values of distance determined during segments of traces before and after transitions, identified by eye. Records at high loads were not corrected for stretching in k_{motor} because the load presumably extends that linkage to be taut.

smooth. Our instrument resolves distances of this size, but we did not find evidence for significant periodicities near ~4 nm. The earlier work, however, was done before the development of single-motor assays, and beads carried unknown numbers of motors, probably several. It is possible that the shorter spacing, if real, might reflect an effect of multiple heads stepping along neighbouring protofilaments.

Our data from moving beads subjected to trap-induced tensions suggest that speeds are largely unaffected by forces of 1.5 pN, and that single molecules of kinesin can still transport beads against loads up to ~5 pN. These findings seem incompatible with the conclusions of Kuo and Sheetz[30], who reported measuring the 'isometric' force generated by single kinesin molecules at 1.9 ± 0.4 pN. In their experiments, nominally arrested beads continued to move; that is, the isometric condition was not truly fulfilled, but this difficulty alone is probably insufficient to explain the discrepancy.

Finding displacement steps in the movement of kinesin molecules is in many respects analogous to detecting current steps in single-channel recordings of neurons. In both cases, steps reflect underlying motions of individual proteins, and allow one to make meaningful measurements at the level of single molecules. Before the advent of single-channel recording, Johnson (thermal) noise due to the leakage resistance of electrodes prevented the resolution of picoampere-sized current steps. Improved methods for increasing this resistance provided conditions that led directly to step detection[46]. As a result, single-channel recording has produced many insights in molecular neuroscience during the past decade. For mechanoenzymes, brownian (thermal) noise of objects pulled by motors prevented the resolution of nanometre-sized displacement steps. Additional stiffness, coming in our case from the optical trap and its effect on the bead linkage, provides the required reduction in noise, permitting visualization of steps. □

Received 16 July; accepted 27 September 1993.

1. Huxley, H. E. *Science* **164,** 1356–1366 (1969).
2. Squire, J. *The Structural Basis of Muscle Contraction* (Plenum, London, 1981).
3. Bagshaw, C. R. *Muscle Contraction* (Chapman & Hall, London, 1982).
4. Burton, K. *J. Musc. Res. Cell Motil.* **13,** 590–607 (1992).
5. Simmons, R. M. *Curr. Biol.* **2,** 373–375 (1992).
6. Cooke, R. *CRC Crit. Rev. Biochem.* **21,** 53–117 (1986).
7. Kron, S. J. & Spudich, J. A. *Proc. natn. Acad. Sci. U.S.A.* **83,** 6262–6276 (1986).
8. Vale, R. D., Schnapp, B. J., Reese, T. S. & Sheetz, M. P. *Cell* **40,** 559–569 (1985).
9. Ishijima, A., Doi, T., Sakurada, K. & Yanagida, T. *Nature* **352,** 301–306 (1991).
10. Uyeda, T. Q. P., Kron, S. J. & Spudich, J. A. *J. molec. Biol.* **214,** 699–714 (1990).
11. Uyeda, T. Q. P., Warrick, H. M., Kron, S. J. & Spudich, J. A. *Nature* **352,** 307–311 (1991).
12. Howard, J., Hudspeth, A. J. & Vale, R. D. *Nature* **342,** 154–158 (1989).
13. Block, S. M., Goldstein, L. S. B. & Schnapp, B. J. *Nature* **348,** 348–352 (1990).
14. Yang, J. T., Saxton, W. M., Stewart, R. J., Raff, E. C. & Goldstein, L. S. B. *Science* **249,** 42–47 (1990).
15. Toyoshima, Y., Kron, S. J. & Spudich, J. A. *Proc. natn. Acad. Sci. U.S.A.* **87,** 7130–7134 (1990).
16. Yanagida, T., Arata, T. & Oosawa, F. *Nature* **316,** 366–369 (1985).
17. Harada, Y., Sakurada, K., Aoki, T., Thomas, D. & Yanagida, T. *J. molec. Biol.* **216,** 49–68 (1990).
18. Higuchi, H. & Goldman, Y. *Nature* **353,** 352–354 (1991).
19. Spudich, J. A. *Nature* **348,** 284–285 (1990).
20. Gittes, F., Mickey, B., Nettleton, J. & Howard, J. *J. Cell Biol.* **120,** 923–934 (1993).
21. Schnapp, B. J. *Meth. Enzym.* **134,** 561–573 (1986).
22. Ashkin, A., Dziedzic, J. M., Bjorkholm, J. E. & Chu, S. *Optics Lett.* **11,** 288–290 (1986).
23. Block, S. M. in *Noninvasive Techniques in Cell Biology* 375–401 (Wiley-Liss, New York, 1990).
24. Denk, W. & Webb, W. W. *Appl. Optics* **29,** 2382–2390 (1990).
25. Amos, L. & Klug, A. *J. Cell Sci.* **14,** 523–549 (1974).
26. Kamimura, S. *Appl. Optics* **26,** 3425–3427 (1987).
27. Kamimura, S. & Kamiya, R. *J. Cell Biol.* **116,** 1443–1454 (1992).
28. Block, S. M., Blair, D. F. & Berg, H. C. *Nature* **338,** 514–517 (1989).
29. Ashkin, A., Schuetze, K., Dziedzic, J. M., Euteneuer, U. & Schliwa, M. *Nature* **348,** 346–348 (1990).
30. Kuo, S. C. & Sheetz, M. P. *Science* **260,** 232–234 (1993).
31. Simmons, R. M. *et al.* in *Mechanisms of Myofilament Sliding in Muscle* (eds Sugi, H. & Pollack, G.) 331–336 (Plenum, New York, 1993).
32. Wang, C. W. & Uhlenbeck, G. E. in *Selected Papers on Noise and Stochastic Processes* (ed. Wax, N.) 113–132 (Dover, New York, 1954).
33. Happel, J. & Brenner, H. *Low Reynolds Number Hydrodynamics* 322–331 (Kluwer Academic, Dordecht, 1991).
34. Kuo, S. C., Gelles, J., Steuer, E. & Sheetz, M. P. *J. Cell Sci.* suppl. **14,** 135–138 (1991).
35. Gallagher, N. C. Jr & Wise, G. L. *IEEE Trans. Acoust. Speech Sign. Proc.* **29,** 1136–1141 (1981).
36. Oosawa, F. & Hayashi, S. *Adv. Biophys.* **22,** 151–183 (1986).
37. Schnapp, B. J., Crise, B., Sheetz, M. P., Reese, T. S. & Khan, S. *Proc. natn. Acad. Sci. U.S.A.* **87,** 10053–10057 (1990).
38. Gelles, J., Schnapp, B. J. & Sheetz, B. J. *Nature* **331,** 450–453 (1988).
39. Kamimura, S. & Mandelkow, E. *J. Cell Biol.* **188,** 865–875 (1992).
40. Ray, S., Meyhoefer, E., Milligan, R. A. & Howard, J. A. *J. Cell Biol.* **121,** 1083–1093 (1993).
41. Song, Y.-H. & Mandelkow, E. *Proc. natn. Acad. Sci. U.S.A.* **90,** 1671–1675 (1993).
42. Harrison, B. C. *et al. Nature* **362,** 73–75 (1993).
43. Kusnetsov, S. A. & Gelfand, V. I. *Proc. natn. Acad. Sci. U.S.A.* **83,** 8530–8534 (1986).
44. Hackney, D. *Proc. natn. Acad. Sci. U.S.A.* **85,** 6314–6318 (1988).
45. Gilbert, S. P. & Johnson, K. A. *Biochemistry* **32,** 4677–4684 (1993).
46. Sakmann, B. & Neher, E. *Single-Channel Recording* (Plenum, New York, 1983).
47. Weingarten, M. D., Suter, M. M., Littman, D. R. & Kirschner, M. W. *Biochemistry* **13,** 5529–5537 (1974).
48. Schnapp, B. J. & Reese, T. S. *Proc. natn. Acad. Sci. U.S.A.* **86,** 1548–1552 (1989).
49. Glatter, O. & Kratky, H. C. *Small Angle X-Ray Scattering* (Academic, New York, 1982).

ACKNOWLEDGEMENTS. We thank W. Denk, C. Godek, M. Meister, P. Mitra and R. Stewart for discussions and advice, W. Hill for electronic design, and R. Stewart for help with motility assays and protein purification. This work was supported by the Rowland Institute for Science (K.S., C.F.S., S.M.B.), and partial support from the NIH (K.S. and B.J.S.), the Lucille P. Markey Charitable Trust (B.J.S.), and the University of Michigan (C.F.S.).